

# Modeling Brownian Motion As A Timelapse Of The Physical, Persistent, Trajectory

*Ludovico Cademartiri*

*Department of Chemistry, Life Sciences and Environmental Sustainability, University  
of Parma, Parco Area delle Scienze 17 A, Parma, Italy*

*ludovico.cademartiri@unipr.it*

## **Abstract**

While it is very common to model diffusion as a random walk by assuming memorylessness of the trajectory and diffusive step lengths, these assumptions can lead to significant errors. This paper describes the extent to which a physical trajectory of a Brownian particle can be described by a random flight.

Analysis of simple timelapses of physical trajectories (calculated over collisional timescales using a velocity autocorrelation function that captures the hydrodynamic and acoustic effects induced by the solvent) gave us two observations: (i) subsampled trajectories become genuinely memoryless only when the time step is  $\sim 200$  times larger than the relaxation time, and (ii) the distribution of the step lengths has variances that remain significantly smaller than  $2Dt$  (usually by a factor of  $\sim 2$ ).

This last fact is due to the combination of two effects: diffusional MSD is mathematically superballistic at short timescales and subsampled trajectories are moving averages of the underlying physical trajectory. In other words, the MSD of the physical trajectory at long time intervals asymptotically approaches  $2Dt$ , but the MSD of the subsampled steps does not, even when the associated

time interval is several hundred times larger than the relaxation time. I discuss how to best account for this effect in computational approaches.

## Introduction

Ensembles of objects in liquids play a major role in questions of great practical and fundamental importance: how does the nucleation of crystals occur? how do proteins fold and interact with ligands, surfaces, and each other? how does diffusion work in crowded environments? A *trait d'union* of these questions is dynamics, i.e., how do those objects move under mutual influence and give rise to collective effects?

One of the challenges with the study of such ensembles is that, on one hand, they are often too numerous and composed of objects too large to be conveniently described at an atomic scale<sup>1-3</sup>; on the other hand, they are often composed of objects too small to be accurately described by most Brownian dynamics approaches<sup>4</sup>. One strategy to approach this problem is to make computation at the atomic scale more efficient<sup>5</sup> or to find better approximations of mean fields<sup>6</sup>. Another strategy, which I espouse here, is to make Brownian descriptions more accurate and practical with smaller objects<sup>7</sup>.

As part of my interest in understanding the diffusional dynamics of ensembles, I looked for approaches to Brownian dynamics simulations of large molecules/nanoparticles in a way that captures the correlations in the system better than conventional memoryless random walk approaches: this paper is the account of that work.

In summary (cf. Figure 1), I first calculate a “physical trajectory”, defined here as the trajectory of a Brownian particle calculated at collisional timescales and that considers most correlation effects. Then I take a “timelapse” of this trajectory at time intervals that are small multiples of the relaxation times. The result is a coarser-grained trajectory, a flight whose autocorrelation functions are “steep” enough to easily provide the autoregression coefficients. These coefficients are what then allows to easily generate ex novo trajectories that encode the correlations of the real, physical trajectory.

Particles in liquid solutions display a spontaneous net displacement over time. Lucretius already intuited in 58 BC that this motion was evidence of the existence of atoms<sup>8</sup>, but it took nearly 2000 years to develop a sound theory of it<sup>9-11</sup>. This motion is subject to a set of conditions: (i) potential gradients are finite, i.e., forces are finite, i.e., accelerations are finite, i.e., the trajectory must be continuous;

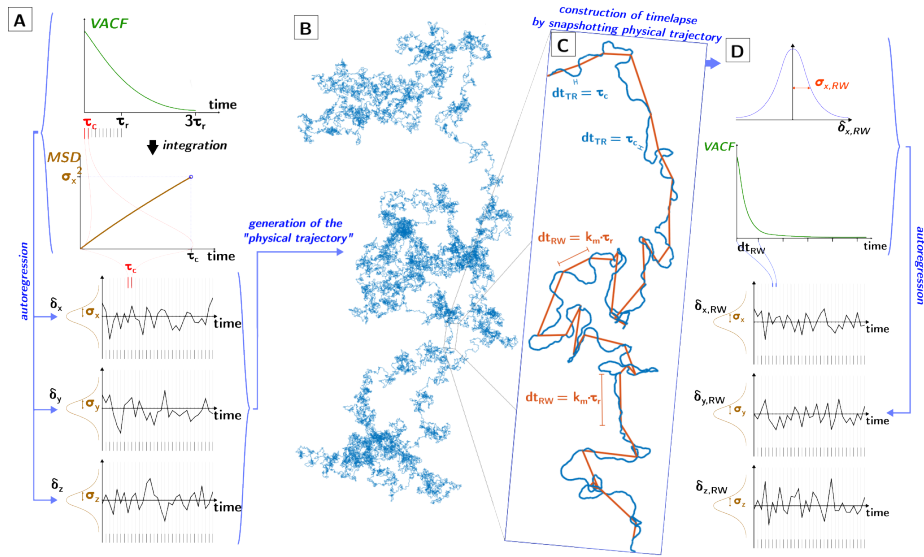


Figure 1: **Timelapse of the physical trajectory.** (A-B) *Generation of the physical trajectory.* From the top down, VACF is calculated up to  $3\tau_c$  on  $\tau_c$  intervals. The MSD at  $\tau_c$  is calculated from a finely integrated VACF from 0 to  $\tau_c$ . The autoregression (AR) coefficients of the long-term VACF, together with the MSD at  $\tau_c$  are used to generate autocorrelated time series of the cartesian components of the displacement  $\delta_x$ ,  $\delta_y$ ,  $\delta_z$  at  $\tau_c$  intervals. (B-C) *Construction of the timelapse.* As the physical trajectory is generated (blue line), snapshots are taken at time intervals  $\tau_K$  integer multiples of  $\tau_r$ . The assembled timelapses constitute a segmented path (orange line). (C-D) *Analysis of timelapse.* The timelapse is analyzed as a persistent random flight, extracting the MSD and VACF. From those, the autoregression coefficients are finally obtained which allow for the rapid generation ex novo of persistent random flights that accurately match the physical trajectory.

(ii) the mass of each particle in the liquid is finite and typically larger than that of the individual liquid molecules surrounding it, i.e., motion is to some degree inertial; (iii) kinetic energy is Maxwell-Boltzmann-distributed, consistently with the laws of thermodynamics and the equipartition theorem; (iv) the structure of liquid solutions is dynamic, disordered in space but homogeneous and isotropic over time, and everything is effectively “in contact” with its neighbors; (v) energy barrier confining a particle in a position of the liquid is finite; (vi) thermal motion is uncorrelated. Based on these facts and assumptions, a particle suspended in a liquid does not oscillate in place but rather diffuses, i.e., its root mean square (RMS) displacement grows with time.

In what follows I only consider spherical objects in the absence of advective flows. Non-sphericity and shear introduce significant complications in the description of motions, collisions, and viscosity<sup>12-15</sup>. For convenience I also describe the distinct objects that make up the liquid as “solvent molecules” (even though there is no requirement for them to be molecules), and the object being moved by collisions with the solvent molecules as the “particle” (even though there is no requirement for it to be a solid phase and not a molecule).

The motion of particles in solution is characterized by two distinct timescales<sup>16-19</sup>.

**Collision time.** The “collisional” timescale is defined here as the mean time that separates two solvent/particle “collisions”. As there are no real collisions in liquids (nearest neighbors are always “in contact”), by “collision” I intend here any transfer of momentum between two neighboring particles caused by orbital overlap. I estimate the mean time between solvent/particle collisions by using a simple logic.

If I assume a weakly interacting liquid with a structure close to random close packing the average number of solvent molecules in contact with the particle is  $\sim 0.886 \cdot (\frac{r_p}{r_s})^2$ , where  $r_p$  is the radius of the particle,  $r_s$  is the radius of a solvent molecule, and 0.886 is the packing fraction for a random close-packed arrangement of circles on a surface<sup>20</sup>.

Any displacement that could trigger a transfer of momentum by “contact” must cause a sufficient overlap between atomic orbitals and therefore should be in the order of an atomic radius, i.e.  $\sim 1 \text{ \AA}$ . Therefore, I am assuming the absence of ions and electrolytes that can interact over large distances. For each solvent molecule on the surface of the particle, the RMS time it takes to move by  $1 \text{ \AA}$  is:

$$\frac{1 \cdot 10^{-10}}{v_{\text{RMS}}} = \frac{1 \cdot 10^{-10}}{\sqrt{\frac{3k_B T}{m_s}}}$$

Where  $v_{\text{RMS}}$  is the RMS velocity of the solvent molecules,  $k_B$  is Boltzmann constant,  $T$  is the temperature and  $m_s$  is the mass of a solvent molecule.

Considering that during this time a solvent molecule can move towards the particle or away from it, and that the particle can also move causing a collision with  $\frac{1}{2}$  of the particles on its surface, the frequency  $f_c$  of collisions between the solvent molecules on the surface and the particle can be estimated as

$$f_c \approx \frac{\sqrt{3k_B T}}{2.26 \cdot 10^{-10}} \left(\frac{r_p}{r_s}\right)^2 \left(\frac{1}{\sqrt{m_s}} + \frac{1}{\sqrt{m_p}}\right) \quad (2)$$

Which means that the mean time  $\tau_c$  between two consecutive solvent/particle collisions can be estimated as its inverse

$$\tau_c \approx \frac{2.26 \cdot 10^{-10}}{\sqrt{3k_B T}} \left(\frac{r_s}{r_p}\right)^2 \left(\frac{\sqrt{m_s m_p}}{\sqrt{m_s} + \sqrt{m_p}}\right) \quad (3)$$

This timescale is most important: if one wants to describe the effect of these solvent/particle collisions as an effective viscous force, one needs to consider timescales  $\gg \tau_c$  so that the number of collisions occurring at each step is large enough to give a stable mean effect.

The largest contributor to  $\tau_c$  is the size of the particle, with the physical properties of the solvent and the temperature being minor effects (cf. Figure S1).

**Relaxation time.** While  $\tau_c$  tells us at what timescales we can make a continuum approximation of the solvent’s viscous drag, the effect that each solvent/particle collision has on the dissipation of the momentum of the particle must depend on its inertia and, therefore, on its density.

In the first order approximation in which the viscous force  $\chi$  acting on the particle is proportional to its velocity, the decay of particle’s momentum occurs exponentially with a decay constant  $\tau_r$ , called the “relaxation time”<sup>19</sup>,

$$\tau_r = \frac{m_p}{\chi}; \quad \text{for spheres: } \tau_r = \frac{2}{9} \frac{\rho_p}{\eta} r_p^2 \quad (4)$$

where  $\rho_p$  is the particle density and  $\eta$  is the dynamic viscosity of the solvent. This relaxation time quantifies the timescale over which the momentum of the particle is dissipated/decorrelated (both in direction and magnitude) by the collisions with the solvent molecules.

These two timescales have opposite dependencies on the size of the particle:  $\tau_c$  goes with  $r_p^{-2}$  while  $\tau_r$  goes with  $r_p^2$ . This fact implies that, depending on the solvent and on the density of the particles, there is a particle radius below which the approximations I have made so far cease to make physical sense (cf. Figure S2). Physically speaking, below a certain particle size (and hence, mass) it takes very few collisions with the solvent molecules, even one, to significantly dissipate the momentum of the particle. In these conditions viscosity cannot describe dissipation, Equation 4 ceases to be valid, and a full collisional description of the system is required. This critical particle radius (cf. Figure S2) lies in the nanoscale for the most common solvents and solid phases.

**The random flight approximation.** In most computational and theoretical studies of Brownian motion the motion of the particles is approximated as a random flight whose steps occur over fixed time intervals<sup>21,22</sup>. Therefore, the choice of the time interval is crucial.

Beside  $\tau_r$  and  $\tau_c$ , there is a third timescale that is often employed in the modeling of ensembles of Brownian objects, which is the time  $\tau_e$  it takes for the RMS displacement (usually assumed to be diffusive) to equal a radius of the particle under consideration (i.e., for spheres,  $\tau_e = r_p^2/6D$ ).

As I show here, while it is correct to assume that, for a Brownian particle (i.e., one for which  $\tau_r \gg \tau_c$ ), the VACF has fully disappeared over  $\tau_e$  (i.e., it is legitimate to use a non-persistent random flight over such timescales), it is quite incorrect, even at such timescales, to use a gaussian distribution with  $2Dt$  variance to describe the cartesian components of the steps. The real step lengths are quite a bit shorter because of the effect of autocorrelation at short timescales (i.e., ballistic motion is mathematically subdiffusive at short enough timescales: the diffusive velocity  $\frac{\sqrt{6D}}{t} \rightarrow \infty$  as  $t \rightarrow 0$ ).

If one chooses (e.g., to consider effects of shape) to look at finer timescales of motion (timesteps in the order of small multiples of  $\tau_r$ ) the autocorrelation must be considered explicitly and its effect on the trajectory is nontrivial.

## Computational Design

**Computational parameters.** Our simulations were conducted considering a library of relevant solvents (H<sub>2</sub>O, EtOH, toluene, tetrachloroethylene, and hexadecane) and particle phases (proteins, amorphous SiO<sub>2</sub>, calcite, Fe<sub>3</sub>O<sub>4</sub>, CdSe, and Au) and particle radii  $r_p$  between  $1.66 \cdot 10^{-10}$  m and  $1 \cdot 10^{-8}$  m in 10 logarithmically distributed steps.

Out of all possible combinations of these parameters, I excluded from consideration those for which  $m_s > m_p$  or  $\tau_r < 10 \cdot \tau_c$ . This last condition ensures that at least 10 solvent/particle collisions are needed to decorrelate the motion of the particle from 1 to  $\sim 1/e$ . Translating this condition in an inequality between the properties of particle and of the solvent molecules the condition leads to

$$\rho_p \cdot r_p^4 \gtrsim 1.098 \cdot 10^{-8} \frac{\eta_s^2}{v_{\text{RMS},s}} = \Gamma_K \quad (5)$$

The right side of the inequality is a temperature-dependent property of the solvent ( $\Gamma_K$ , in [Kg · m]) that can be easily tabulated for reference (cf. Table I)

**Table I.**

Solvent	Temperature [°C]	$\Gamma_K$ [ $10^{-33}$ kg · m]
Water	25	0.419
	70	0.391
Toluene	25	1.95
Ethanol	25	1.77
Tetrachloroethylene	25	3.75
Hexadecane	25	32.5
	300	23.5

Using these values it is easy to estimate the smallest particle radius  $r_B$  that could be reasonably described by a Brownian simulation (with the possible caveat of having to consider autocorrelation effects). For a SiO<sub>2</sub> particle in water  $r_B$  is 0.654 nm, for CdSe in hexadecane at 300 C (close to synthesis conditions for colloidal quantum dots)  $r_B$  is 0.693 nm, while for Au particles in water is 0.384 nm. Importantly, for a protein in water at room temperature (considering a molecular-weight independent density of  $1220 \text{ Kg/m}^3$ <sup>23</sup>)  $r_B$  is  $\sim 0.76$  nm, smaller than most proteins.

Figure 2A shows  $r_B$  as a function of  $\rho_p$  at 298K. The data for the plot were calculated accounting for the variation of  $\eta$  (through Andrade<sup>24,25</sup> and Vogel<sup>26</sup> equations using parameters from Reid, Prausnitz & Poling<sup>27</sup>) and  $\rho_s$  (through Hankinson-Brobst-Thomson technique<sup>28</sup> using parameters also from Reid, Prausnitz & Poling<sup>27</sup>) with T.

Brownian dynamics *can*, in principle, be used to describe the motion in liquids of nearly everything but small molecules.

**The “physical” trajectory.** Simulations are discrete by their own very nature. The smallest “discontinuities” in the motion of the particles in solution are the individual collisions with the solvent molecules. This means that choosing  $\tau_c$  as the discrete time step used in calculating this “physical” trajectory seems reasonable (cf. Figure 1A). Once determined the timescale, all one needs to calculate the trajectory, in theory, is a suitable VACF.

*The distribution of the displacement magnitudes of the physical trajectory.*

The mean squared displacement  $\sigma_x^2$  as a function of time can be obtained directly from the VACF by

$$\sigma_x^2(t) = 2 \int_0^t (t - \tau) C_v(\tau) d\tau \quad (6)$$

where  $C_v$  is the non-normalized VACF<sup>29</sup>.

The VACF decays exponentially only if caused by random noise. In reality, the interaction with the surrounding liquid during motion is not uncorrelated<sup>30</sup>. Firstly, as the particle moves into the liquid, it “writes” information about its own passage into the dynamics of the liquid itself: vortices (i.e., a collective, correlated motion of the liquid molecules) are created in the wake of the particle. A particle moving inside this correlated velocity field is inevitably correlated with its own past motion. The correlation vanishes in time as these vortices propagate away from the particle over the “vorticity diffusion time”,  $\tau_v = \frac{\rho_s}{\eta} r_p^2$ , where  $\rho_s$  is the density of the liquid.

The second effect is due to the compressibility of the liquid, which causes it to undergo compression when the particle pushes against it. This compression establishes acoustic waves in the liquid that affect the velocity field of the liquid surrounding the particle at later times. The timescale of this process is the sonic time  $\tau_s = \frac{r_p}{c}$ , where  $c$  is the speed of sound in the liquid.

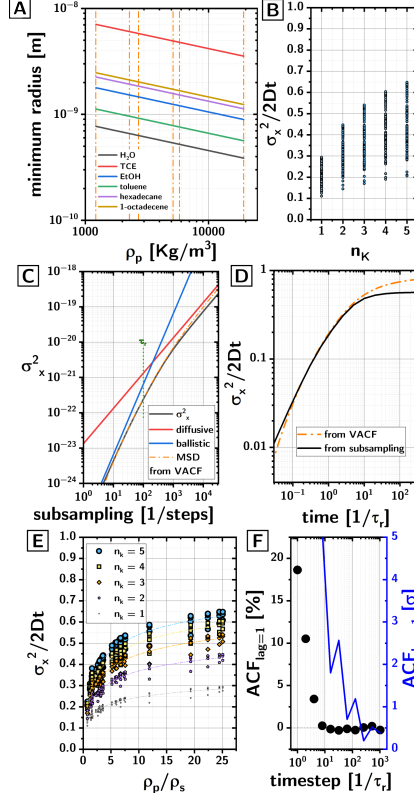


Figure 2: **(A)** Minimum radius of particles describable as Brownian (i.e.,  $\tau_T > 10\tau_c$ ), as a function of their density, their phase, and the solvent. **(B)** Ratio between the observed variance of the step length  $\sigma_x^2$  (single cartesian coordinate) in the timelapse and the diffusional prediction  $2Dt$ . The ratio is plotted as a function of the time resolution of the timelapse (physical trajectory is sampled at  $\tau_K = n_K \cdot \tau_T$  time intervals). **(C)** Variance of the step length  $\sigma_x^2$  from our timelapse (black line), compared to the diffusive MSD (red), ballistic MSD (blue), and the MSD obtained from the VACF of the physical trajectory (orange dash dot). The data is plotted as a function of the time interval. The MSD obtained from the VACF transitions from ballistic to diffusive regimes around the relaxation time  $\tau_T$ , but the variance of the step length  $\sigma_x^2$  from the timelapse remains offset from the diffusional prediction at long times. **(D)** Same data as panel C but plotted in terms of the ratio between the MSD and the diffusional prediction. **(E)** Ratio between the MSD and the diffusional prediction as a function of the density ratio ( $\rho_p/\rho_s$ ) and the subsampling rate. **(F)** Decorrelation at lag=1 as a function of the timestep in the timelapse (in units of  $\tau_T$ ), expressed either as percentage of autocorrelation (black scatters) or as standard deviations from the mean autocorrelation at large lags (blue).

These two effects are usually somewhat separated in timescale (typically  $\tau_s < \tau_v$ , cf. Figure S3A), so they are accounted for by a VACF composed of two terms that dominate respectively at long and short timescales<sup>30-34</sup>:

$$C_v(t) = \frac{k_B T}{M} \left\{ \frac{2\rho_p}{9\pi\rho_s} \int_0^\infty \frac{\sqrt{x} e^{-\frac{x t}{\tau_v}}}{1 + \sigma_1 + \sigma_2 x^2} dx + \frac{e^{-\frac{\alpha_1 t}{\tau_s}}}{1 + \frac{2\rho_p}{\rho_s}} \left[ \cos\left(\frac{\alpha_2 t}{\tau_s}\right) - \frac{\alpha_1}{\alpha_2} \sin\left(\frac{\alpha_2 t}{\tau_s}\right) \right] \right\} \quad (6)$$

where  $\sigma_1 = \frac{1}{9} \left(7 - 4 \frac{\rho_p}{\rho_s}\right)$ ,  $\sigma_2 = \frac{1}{81} \left(1 + 2 \frac{\rho_p}{\rho_s}\right)^2$ ,  $\alpha_1 = 1 + \frac{\rho_s}{2\rho_p}$ ,  $\alpha_2 = \sqrt{1 - \left(\frac{\rho_s}{2\rho_p}\right)^2}$ , and  $M$  is the ‘‘effective mass’’ of the particle  $M = \frac{4}{3} \pi r_p^3 \left(\rho_p + \frac{\rho_s}{2}\right)$ : a particle moving a liquid must displace liquid to do so which means that its mass must include the mass of the displaced liquid.

To generate the physical trajectory, I calculated this VACF for each combination of solvent and particle up to times equal to  $3 \cdot \tau_r$  in time intervals equal to  $\tau_c$ . The MSD,  $\sigma_x^2$ , at the time  $\tau_c$  (i.e., the timestep chosen for the physical trajectory) was calculated from the same VACF, but integrated with a much finer time resolution ( $\tau_c/10^4$ ) given the sensitivity of the integral in Equation 4 to the discretization (cf. Figure 1A). The calculated VACF follows the expected power law tail with a -3/2 exponent (Figure S3B).

*The persistence of motion.*

A more delicate process is the determination of the displacements for each timestep, since these have to be autocorrelated according to the  $C_v(t)$  I just described. To do so, it is necessary to determine the autoregression coefficients  $\beta_i$  for the expansion

$$v_x(t) = \sum_{i=1}^l \beta_i v(t-i) + \xi(t) \quad (7)$$

where  $v_x(t)$  is the  $x$  component of the velocity at the step  $t$ ,  $\xi(t)$  is the noise function, and  $l$  is the maximum lag being considered (in our case  $3\tau_r/\tau_c$ ). The coefficients were calculated by solving the corresponding Yule-Walker system of equations expressed in terms of the autocorrelation function

$$\begin{pmatrix} C'_1 \\ C'_2 \\ C'_3 \\ \vdots \\ C'_l \end{pmatrix} = \begin{bmatrix} C'_0 & C'_1 & C'_2 & \dots \\ C'_1 & C'_0 & C'_1 & \dots \\ C'_2 & C'_1 & C'_0 & \dots \\ \vdots & \vdots & \vdots & \ddots \\ C'_{l-1} & C'_{l-2} & C'_{l-3} & \dots \end{bmatrix} \begin{pmatrix} \beta_1 \\ \beta_2 \\ \beta_3 \\ \vdots \\ \beta_l \end{pmatrix} \quad (1)$$

where the left side is the vector of the normalized autocorrelation function  $C'$  (subscripts indicating the lag as number of time intervals  $\tau_c$ ), while the right side is the product of the Toeplitz matrix of  $C'$  (from lag 0) and the vector of the autoregression coefficients<sup>35,36</sup>.

This brute force approach is not without challenges: for the coefficients obtained from  $C'$  to generate a time series with autocorrelation close to  $C'$  it is necessary for the input  $C'$  to be highly precise (i.e., integration of the VACF must be done with small  $dx$  intervals). Since many of our simulations involve lags in excess of  $10^5$  timesteps, solving the system of equations in double precision can be cumbersome (since I am modeling one particle at a time, the matrices are large but I could not make GPU processing in double precision advantageous). Estimation approaches such as the Durbin-Levinson did not give me coefficients able to reproduce the desired autocorrelation in the produced time series<sup>37</sup>. Using this approach, the VACF of the physical trajectory produced using the autoregression coefficients as described above match closely the input VACF (cf. Figure S3C).

Once I determined the  $\beta_i$  coefficients, the individual components of the displacements were generated as a timeseries of unitary variance by scaling the noise term  $\xi(t)$  by a factor  $\sigma_n = \sqrt{1 - C' \cdot \beta}$ , where the dot indicates a dot product of the  $C'$  and  $\beta$  vectors. The resulting time series of the individual components of the 3D displacement shows the expected variance and distribution (cf. Figure S3D). The time series is then scaled to obtain the variance consistent with  $\sigma_x^2$  (cf. Figure 1A).

This process is executed for each spatial component, obtaining independent timeseries for the individual components of the displacement (cf. Figure 1A-B), which are then assembled as displacement vectors, and their cumulative sum is the final trajectory.

The distribution of the lengths of the 3D displacement vectors follows expectedly a Maxwell-Boltzmann distribution (cf. Figure S3E). The RMS velocities obtained

from these distributions are close to the ballistic values as expected from the fact that the timestep of the physical trajectory is  $\tau_c$  (cf. Figure S3F). The difference from the ballistic values depends on the relative solvent/particle compositions and especially on their density ratio as it determines the decorrelation impact associated with each solvent/particle collision. Lastly, the orientations of the displacements that make up the physical trajectory, sampled over a long enough time, appear to be ergodic (cf. Figure S3G).

The autocorrelation functions at lag=1 associated with the physical trajectory are not identical (cf. Figure S3H for an example). The autocorrelation of the moduli of the displacement vectors is lower than that for the individual components, while the autocorrelation of the orientation of the displacement vectors is also lower than that for the cartesian components of the displacements but higher than for the moduli. In other words, the orientation of motion is more strongly autocorrelated at short times than the lengths of the steps.

**Subsampling into a random flight.** While calculating the physical trajectory (cf. Figure 1B for an example of a small section of a calculated trajectory), I took “snapshots” of the particle positions at intervals of time  $\tau_K$  where  $\tau_K = n_K \cdot \tau_r$ , where  $n_K$  is an integer I call the “Kuhn multiplier” (in our simulations  $\tau_K$  was between 1 and 5). The name “Kuhn multiplier” is an homage to Prof. Werner Kuhn who applied a reasoning similar to this to describe the conformation of polymers as random flights with the goal of calculating their conformational entropy<sup>38</sup>.

As these snapshots separated by time intervals  $\tau_K$  are compiled, the positions of the particle in those snapshots form what looks like a random flight that is a coarser-grained (i.e., subsampled), but accurate representation of the physical trajectory (cf. Figure 1).

In a sense this is the opposite conceptual approach that Prof. Kuhn took. I am not creating random flights of fixed step length and try to find at which value of step length the overall conformation of the polymer is described by the random flight. I am taking the physical trajectory, snapshot it at fixed time intervals, and find out what kind of random flights are generated as a result.

For such extracted random flights to be then separately reproduced *ex novo* as a coarse-grained model of a physical Brownian trajectory, they should be then characterized for: (i) their step length distribution; (ii) their autocorrelation and autoregression coefficients. In what follows I describe how these functions change as a function of solvent, material and size of the particle, as well as  $n_K$ .

## Results and Discussion

It could be tempting to think that the MSD, VACF and other quantities associated with the timelapse would be just the values of MSD and VACF from the physical trajectory at longer times. This is not the case. Subsampling changes the autocorrelation of a timeseries in often unpredictable ways, even if the overall conformation of the trajectory is preserved<sup>39</sup>. This can be understood in terms of Fourier transforms: a subsampling is a low-pass filter that “forgets” high frequency correlations in a way that depends subtly on the structure of the VACF (which is why I could not just calculate the MSD at  $t = \tau_K$ ).

The timelapses are essentially somewhat persistent random flights where the steps are equispaced in time by a multiple of the relaxation time of the system. To characterize these flights we have to look at the distribution and mean squared values of the displacements, and the ACFs of the displacements.

The distributions of the single component displacements in the timelapse were exceedingly well fitted with normal distributions ( $R^2$  across all our conditions was  $0.9993 \pm 0.0001$ ), and the displacement step acceptably well described by Maxwell-Boltzmann distributions ( $R^2 = 0.998 \pm 0.01$ ).

There are two noteworthy observations.

The first is that the  $\sigma_x^2$  of the subsampled steps are distinctly subdiffusive in absolute value (the exponent of the dependence on time is instead diffusive) even when the snapshots are taken every  $5\tau_r$  (cf. Figure 2B, the single step  $\sigma_x^2$  (averaged across all our simulations) was 0.44 times the diffusive value when  $n_k=5$ , i.e., when motion is often regarded as diffusive. This is not necessarily surprising for at least two reasons: (i) at very short timescales even ballistic motion is, mathematically speaking, “subdiffusive” and (ii)  $\sigma_x^2$  of a subsampled time series are basically moving averages with a window as wide as the time interval, hence they “lag” the continuous time series they derive from.

It is easy to show how, for an identical trajectory, the  $\sigma_x^2$  for a single step depends on its subsampling. A single physical trajectory was calculated for  $10^9$  steps corresponding to  $\tau_c$  and where  $\tau_r \cong 100\tau_c$ . The trajectory was then subsampled every 2, 4, 8 steps and so on, up to 32768 steps. The variance of the Gaussian distribution of the single components of the displacements (i.e., the  $\sigma_x^2$ ) in these subsamplings can be then compared with the diffusive and ballistic MSD obtaining the plot in Figure 2C. Importantly, the dash-dot orange curve in Figure 2C shows the MSD one could have calculated directly from the VACF at

the corresponding time intervals. The discrepancy between the MSD from the subsampling and that from the VACF becomes very significant for subsamplings larger than  $\tau_r$ .

Furthermore, the ratio between the variance  $\sigma_x^2$  of the distribution of single step displacements of the subsampled trajectory and  $2Dt$  is different from what one would obtain directly from the VACF in Eq. 5 (cf. Figure S2D). The  $\sigma_x^2$  derived directly from the VACF tends asymptotically to  $2Dt$  as  $t$  increases, while the one obtained from subsampled trajectories plateaus to a value that is significantly lower than  $2Dt$ .

This means that picking a time interval for a Brownian simulation that is orders of magnitude larger than  $\tau_r$  does not lead to a diffusive step length as it is usually assumed on the basis of the relationship between VACF and MSD. Making that approximation causes a very significant overestimate of the step lengths of the random walk.

The second noteworthy thing is the large spread in the values of  $\sigma_x^2/2Dt$  for identical values of  $n_k$ . This could be surprising or not depending on the reason why it happens. It could be because of (i) insufficient statistics on the simulations, (ii) excessively coarse integration of the VACF or premature truncation of it, or (iii) something intrinsic to the model.

The first two hypotheses were easily disproven. First,  $\sigma_x^2$  calculated from 1000 replicate trajectories gave relative standard errors on the mean of  $10^{-4}$ : the values are reproducible. Second, extending the calculation of the VACF to  $100\tau_r$  and decreasing the size of the  $dx$  interval in Eq. 5 by three orders of magnitude did not change the  $\sigma_x^2$  significantly (certainly less than 1%): it is not a problem with the numerical integration.

The explanation for the spread is hinted at by the fact that the  $\sigma_x^2/2Dt$  ratio appears to be dependent on the density ratio  $\rho_p/\rho_s$  (cf. Figure 2E), without explaining fully the spread. The density ratio is featured prominently in Eq. 5 which quantifies the VACF. The VACF in Eq. 5, as already stated, does not decay exponentially. Nonetheless, the  $\tau_r$  on which I base the subsampling intervals is obtained from Eq. 4 which assumes an exponential decay of the VACF. Furthermore, the subsampling intervals I picked in order to allow for the study of small Brownian particles, are in a range where the  $\sigma_x^2/2Dt$  ratio is still rapidly changing (cf. Figure 2D). Taken together, these facts indicate that the spread of the values in Figure 2B are the result of (i) the difficulty of quantifying a relaxation time for an algebraic decay curve (i.e.,  $\tau_r$  corresponds

to different degrees of decorrelation depending on the density ratio and other physical variables used in Eq. 5), (ii) the steep dependence of the  $\sigma_x^2/2Dt$  ratio on time for subsampling intervals of small multiples of  $\tau_r$ .

An unfortunate consequence of this spread is that the VACF for the subsampled random flight must be probably calculated before each simulation.

Lastly but importantly: using the correct  $\sigma_x^2$  for the timestep chosen can be sufficient in generating accurate *ex novo* trajectories. To assess how quickly the autocorrelation vanishes as a function of the subsampling we calculated the autocorrelation of the 1D components of the displacements as a function of the subsampling in units of  $\tau_r$  (for the calculation we used the  $10^9$  step physical trajectory mentioned above). This analysis (cf. Figure 2F) shows that autocorrelation at lag=1 vanishes for subsamplings where the timestep is approximately equal to  $32\tau_r$ . If one looks at how the autocorrelation at lag=1 compares to the standard deviation of the autocorrelation at large lags (cf. Figure 2F, blue) then one might want to push to  $200\tau_r$  to ensure complete loss of autocorrelation.

Somewhat surprisingly, in most cases for which  $\tau_r > 10\tau_c$  (i.e., Brownian regime) the condition for memorylessness of the path (timestep =  $200\tau_r$ ) leads to RMS step lengths safely shorter than the diameter of the particles (cf. Figure 3A-E). In other words, a Brownian simulation where the timestep is commensurate to the time it takes the particle to move by its radius can safely ignore autocorrelation. It is obviously important to keep the Brownian step significantly smaller than the particle radius since the steps are normally distributed and Brownian simulations involve often large numbers of steps: steps that are 5+ standard deviations away from the mean cannot be excluded. This fact, especially in the case of highly concentrated systems, can cause issues in the accurate detection of collisions.

In the case in which instead the timestep chosen is a small multiple of  $\tau_r$ , then autocorrelation must be considered. To do so, we took the subsampled trajectories, extracted their VACF, calculated the autoregression coefficients by solving Eq. 7, and then used Eq. 6 to calculate *ex novo* new trajectories. The noise term was normalized to give a variance equal to the  $\sigma_x^2$  extracted from the original subsampled trajectory.

The results of this approach are positive. The VACF obtained from these *ex-novo* trajectories match very closely the VACF of the original subsampled trajectory (cf. Figure 3F for a representative example).

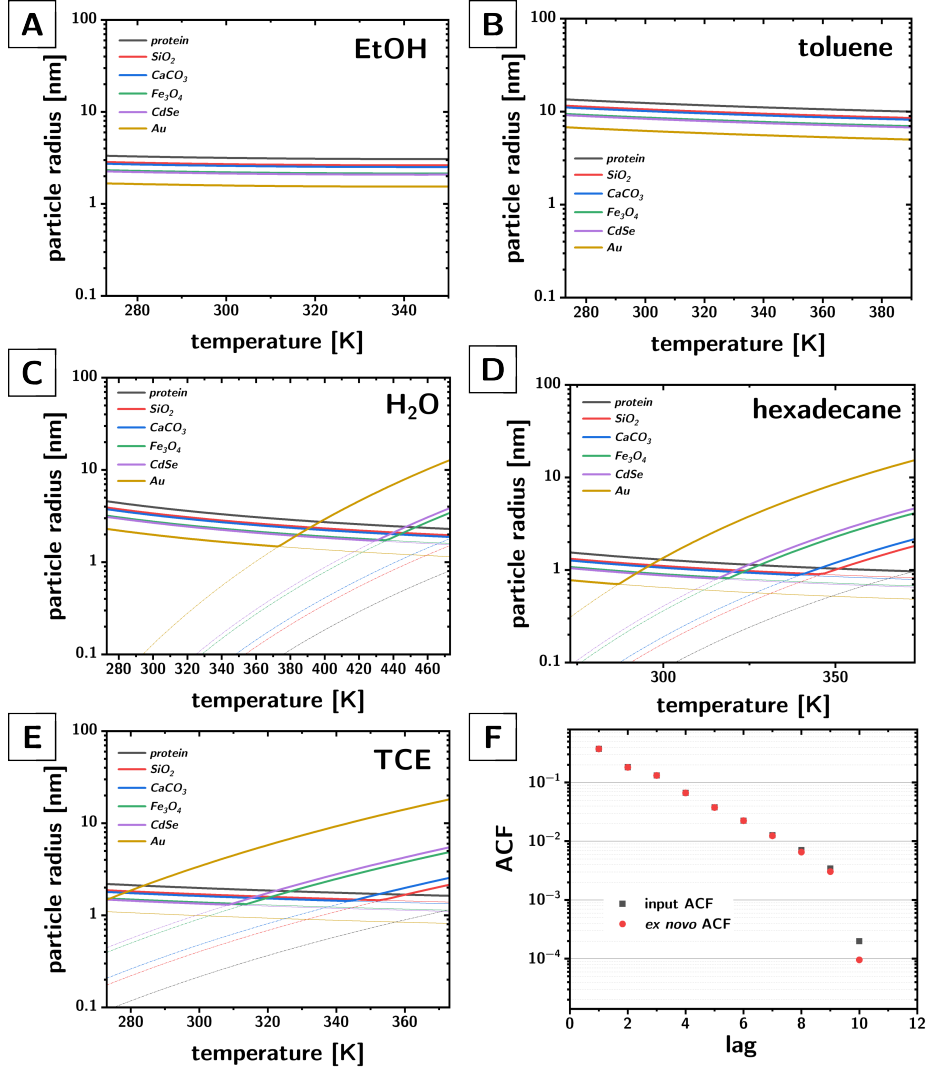


Figure 3: **(A-E)** Minimum particle radii (as a function of particle phase, temperature, and solvent) to satisfy the Brownian regime (thin colored solid lines) and the memorylessness approximation (dash-dotted thin lines), i.e., timesteps long enough to eliminate autocorrelation ( $\tau_K \sim 200\tau_r$ ) produce RMS displacements significantly shorter than the diameter of the particles. **(F)** Representative comparison between the autocorrelation (ACF) obtained from the input trajectory (i.e., the timelapse of the physical trajectory), and from the ex-novo trajectories obtained with the autoregression coefficients extracted from the input ACF.

## Conclusions

In conclusion, I have explored and discussed to what extent a Brownian trajectory can be modeled as a random flight. The reason why I did it is that diffusion is often modeled (especially in simulations of ensembles of particles) as a random flight assuming memoryless trajectories and diffusional step lengths ( $\sigma_x = (2Dt)^{1/2}$ ) on top of which corrections are then made to account for interactions. As I show here, the first approximation can be often reasonable, but the second is fundamentally wrong and leads to a very significant overestimation of the step lengths,

To find this, I have (i) calculated a physical Brownian trajectory by considering collisional timescales and a VACF that accounts for hydrodynamic and acoustic effects, (ii) taken snapshots of particle positions at time intervals that are multiples of the relaxation time, (iii) analyzed the subsampled trajectory as an autocorrelated random flight extracting MSD and VACF.

The simulations (considering a variety of solvents, particle phases, and particle sizes) show that (i) subsampled flights become genuinely memoryless only when the time step is  $\sim 200$  times larger than the relaxation time, and (ii) the distribution of the step lengths is nicely gaussian (on each cartesian component) but with variances that remain significantly smaller than  $2Dt$ . As we discuss, this last fact is due to the combination of two effects: diffusional MSD is mathematically superballistic at short timescales and subsampled trajectories are moving averages of the underlying physical trajectory. In other words, maybe counterintuitively, the MSD of the physical trajectory at long time intervals asymptotically approaches  $2Dt$ , but the MSD of the subsampled steps does not, even when the associated time interval is several hundred times larger than the relaxation time.

Practically speaking, given the inaccuracies of the estimated relaxation times, the appropriate corrections to the step lengths (or, alternatively, to the diffusivities) must be extracted from a simulated physical trajectory, using the physical parameters of the system at hand and the chosen subsampling. The simulations discussed here in fact show that the precise value of the correction depends intimately on the specific physical parameters (densities, radii, etc. . . ) in ways that are not accurately captured by empirical fits.

## Supporting Information

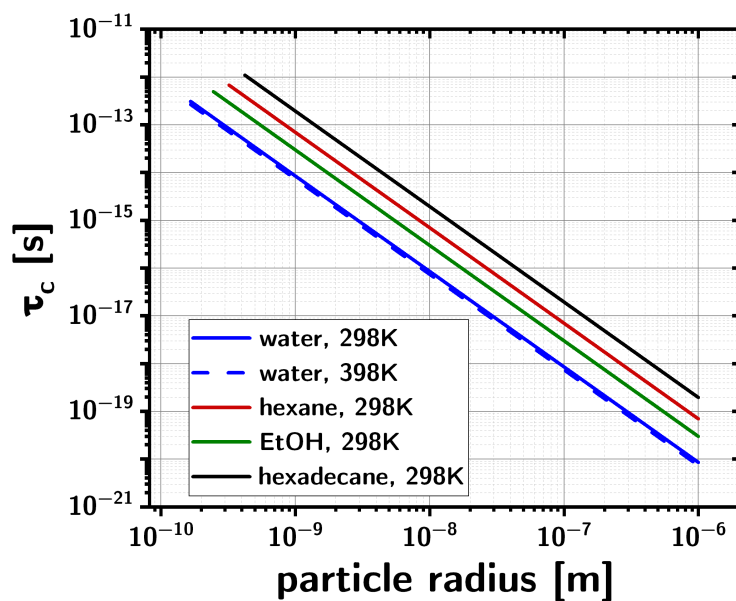
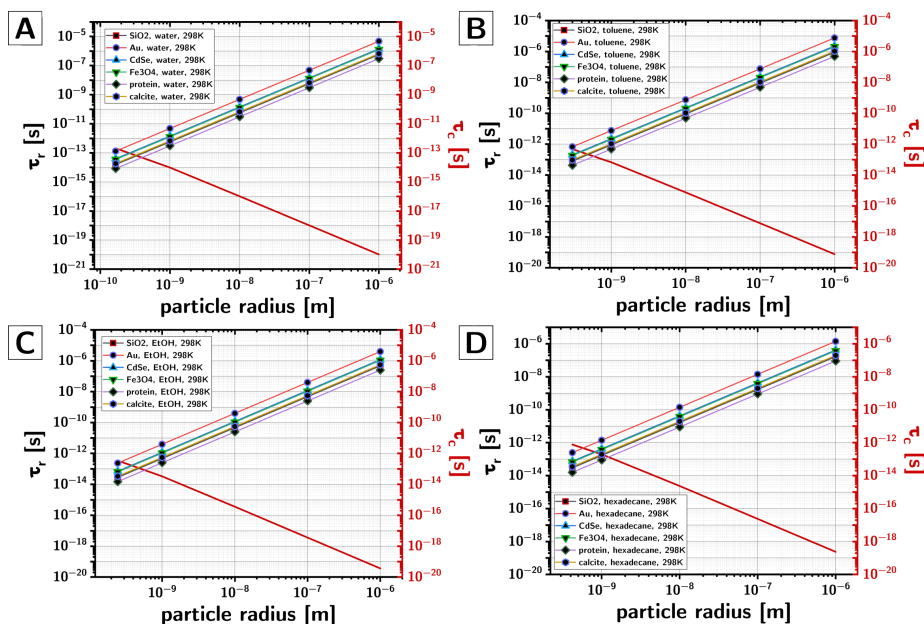
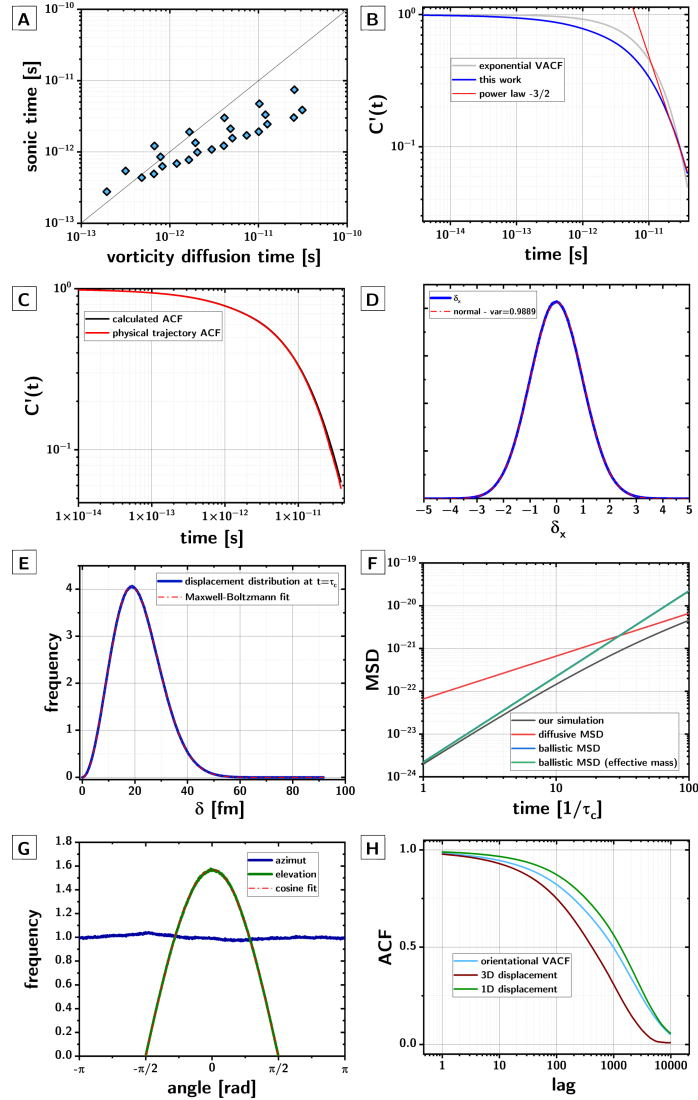


Figure S1. *Collisional timescale as a function of solvent/particle characteristics and temperature.* The calculated value of the collisional timescale  $\tau_c$  (according to Eq. 3) as a function of the particle radius, for a range of solvents, temperatures, and particle phases.



**Figure S2.** *Collisional and relaxation timescales as a function of particle radii, particle phases and solvents.* The graphs overlay, for the same system, the collisional timescale from Eq. 3 (red line, no scatter, scale on the left axis) with the relaxation timescale from Eq. 4 (colored lines, black-filled scatters, scale on the right axis). As discussed in the main text, the validity of the relaxation time formalism (i.e.,  $\tau_r \gg \tau_c$ ) falls apart only when particles are smaller than  $\sim 10^0$  nm, depending on the combination of solvent, particle phase. Data for different solvents are in different panels( water (A), toluene (B), EtOH (C), and hexadecane (D)).



**Figure S3. Computational diagnostics.** **A.** Relation between sonic time and vorticity diffusion time for the simulation parameters explored. **B.** Comparison between normalized VACFs (exponential in grey vs according to Eq. 5 in blue); the red line shows the algebraic decay fit with a -3/2 exponent. **C.** Comparison between the VACF calculated from Eq. 5 (black) and the one derived from the physical trajectory generated from the  $\beta_1$  coefficients (red). **D.** Distribution of the time series of one-dimensional univariant displacements in the physical trajectory (blue) and the gaussian fit (red dashed). **E.** Distribution of the 3D displacements magnitudes in a physical trajectory (blue) and Maxwell-Boltzmann fit (red dashed). **F.** Comparison between the MSD as a function of time (in  $\tau_c$  units) from a physical trajectory derived from the VACF in Eq. 5 (black), from a ballistic motion (blue), ballistic motion accounting for the effective mass (green) and from a diffusive motion (red). **G.** Distributions of azimuths and elevations in the displacement orientations in a physical trajectory. The dependence on the angle of both is consistent with a uniform distribution on the spherical angle. **H.** Comparison of the ACF (at lag=1) calculated from a physical trajectory (orientational in cyan, 3D displacement magnitude in dark red, and 1D displacement magnitude in green)

## References

- (1) Gupta, C.; Sarkar, D.; Tieleman, D. P.; Singharoy, A. *Curr. Opin. Struct. Biol.* **2022**, *73*, 102338.
- (2) Lbadaoui-Darvas, M.; Garberoglio, G.; Karadima, K. S.; Cordeiro, M. N. D.; Nenes, A.; Takahama, S. *Mol. Simul.* **2023**, *49*, 1229.
- (3) Joshi, S. Y.; Deshmukh, S. A. *Mol. Simul.* **2021**, *47*, 786.
- (4) Muñiz-Chicharro, A.; Votapka, L. W.; Amaro, R. E.; Wade, R. C. *Wiley Interdisciplinary Reviews: Computational Molecular Science* **2023**, *13*, e1649.
- (5) Anderson, J. A.; Lorenz, C. D.; Travesset, A. *J. Comput. Phys.* **2008**, *227*, 5342.
- (6) Gkeka, P.; Stoltz, G.; Barati Farimani, A.; Belkacemi, Z.; Ceriotti, M.; Chodera, J. D.; Dinner, A. R.; Ferguson, A. L.; Maillet, J.-B.; Minoux, H. *J. Chem. Theory Comput.* **2020**, *16*, 4757.
- (7) Smith, G. E.; Seth, R. *Brownian motion and molecular reality*; Oxford University Press, 2020.
- (8) Lucretius, T. C. *De rerum natura*, 58 BC.
- (9) Einstein, A. *Ann. Phys* **1906**, *19*, 371.
- (10) Smoluchowski, M. M. *Bulletin International de l'Académie des Sciences de Cracovie* **1906**, 202.
- (11) Perrin, J. B. *Ann. Chim. Phys.* **1909**, *18*, 5.
- (12) Zaccone, A.; Dorsaz, N.; Piazza, F.; De Michele, C.; Morbidelli, M.; Foffi, G. *The Journal of Physical Chemistry B* **2011**, *115*, 7383.
- (13) Pelargonio, S.; Zaccone, A. *Physical Review E* **2023**, *107*, 064102.
- (14) Jain, R.; Sebastian, K. *The Journal of chemical physics* **2017**, *146*.
- (15) Lattuada, M.; Wu, H.; Morbidelli, M. *Langmuir* **2004**, *20*, 5630.
- (16) Selmeczi, D.; Tolić-Nørrelykke, S.; Schäffer, E.; Hagedorn, P.; Mosler, S.; Berg-Sørensen, K.; Larsen, N. B.; Flyvbjerg, H. *Acta Physica Polonica B* **2007**, *38*.
- (17) Huang, R. *Brownian motion at fast time scales and thermal noise imaging*; The University of Texas at Austin, 2008.

- (18) Li, T.; Raizen, M. G. *Annalen der Physik* **2013**, *525*, 281.
- (19) Philipse, A. *Utrecht University, Debye Institute, Van't Hoff Laboratory* **2011**.
- (20) Zaccone, A. *Phys. Rev. Lett.* **2022**, *128*, 028002.
- (21) Chen, J. C.; Kim, A. S. *Adv. Colloid Interface Sci.* **2004**, *112*, 159.
- (22) Huber, G. A.; McCammon, J. A. *Trends in chemistry* **2019**, *1*, 727.
- (23) Andersson, K.; Hovmöller, S. *Zeitschrift für Kristallographie-Crystalline Materials* **1998**, *213*, 369.
- (24) Andrade, E. d. C. *The London, Edinburgh, and Dublin Philosophical Magazine and Journal of Science* **1934**, *17*, 497.
- (25) Andrade, E. d. C. *Nature* **1930**, *125*, 309.
- (26) Vogel, H.; Weiss, A. *Berichte der Bunsengesellschaft für physikalische Chemie* **1982**, *86*, 193.
- (27) Reid, R.; Prausnitz, J. P., BE; McGraw-Hill: 1987.
- (28) Hankinson, R. W.; Thomson, G. H. *AIChE J.* **1979**, *25*, 653.
- (29) Berlinsky, A.; Harris, A. *Statistical Mechanics: An Introductory Graduate Course*; Springer Nature, 2019.
- (30) Chakraborty, D. *The European Physical Journal B* **2011**, *83*, 375.
- (31) Zwanzig, R.; Bixon, M. *Phys. Rev. A* **1970**, *2*, 2005.
- (32) Chow, T.; Hermans, J. *Physica* **1973**, *65*, 156.
- (33) Hinch, E. J. *J. Fluid Mech.* **1975**, *72*, 499.
- (34) Clercx, H.; Schram, P. *Phys. Rev. A* **1992**, *46*, 1942.
- (35) Brockwell, P. J. *Time series: Theory and methods*; Springer-Verlag, 1991.
- (36) Shumway, R. H.; Stoffer, D. S.; Stoffer, D. S. *Time series analysis and its applications*; Springer, 2000; Vol. 3.
- (37) Cybenko, G. *SIAM Journal on Scientific and Statistical Computing* **1980**, *1*, 303.
- (38) Kuhn, W. *Kolloid-Zeitschrift* **1934**, *68*, 2.
- (39) Kennedy, M. C.; Prichard, S. J. *Landsc. Ecol.* **2017**, *32*, 945.